Soft Matter

PAPER



Cite this: *Soft Matter*, 2025, **21**, 458

# Low field electrocaloric effect at isotropic–ferroelectric nematic phase transition†

A. Adaka,[ab] P. Guragain,[d] K. Perera,[ac] P. Nepal,[d] R. J. Twieg[d] and A. Jákli *[abc]

Received 14th August 2024,
Accepted 10th December 2024

DOI: 10.1039/d4sm00979g

rsc.li/soft-matter-journal

Electrocaloric effects (ECE) in solid state materials, such as ferroelectric ceramics and ferroelectric polymers, have a great impact in developing cooling systems. Herein, we describe the ECE of a newly synthesized ferroelectric nematic liquid crystal compound at the isotropic–ferroelectric nematic ($I–N_F$) phase transition. While the Joule heat completely suppressed the ECE in a DC field, in an AC field with $E < 1.2$ V μm$^{-1}$ and $f \geq 40$ Hz, an increase in optical transmittance was observed, which in comparison with a zero-field transmittance *versus* temperature plot indicated a shift in the transition temperature. These findings implied that one can induce the desired phase transition using an electric field *via* ECE with an EC responsivity of $\sim 1.7 \times 10^{-6}$ km V$^{-1}$. Notably, the required electric field was two orders of magnitude smaller than the typical fields for other EC materials. EC effects observed under such low fields is a unique property of ferroelectric nematic liquid crystals. Furthermore, the specific EC energy could be increased considerably by reducing the ionic content, thus suppressing the Joule heat.

## Introduction

Over the years, there have been significant improvements in the applications of various caloric effects, such as mechanocaloric (barocaloric and elastocaloric), magnetocaloric and electrocaloric effects, in environmentally friendly cooling systems and compact and improved efficiency refrigeration.[1–9] Electrocaloric effect (ECE) occurs when an electric field applied in a higher entropy phase (that usually occurs at a higher temperature) of a material reduces the entropy to the level of a lower temperature phase. Therefore, *via* the application of an electric field, ECE brings about a reversible entropy change in the material, leading to heat exchange within the environment.[10–14]

Solid state ECE materials typically have either high dielectric permittivity or switchable macroscopic polarization (ferroelectric), which result in strong coupling in the applied electric fields. In the case of a material with paraelectric (P)–ferroelectric (F) phase transition on cooling, the electric field aligns with the molecular dipoles toward the field corresponding to the ferroelectric phase, thus reducing the entropy to the level of the F phase.

In ECE materials, reversible isothermal entropy change $\Delta S = \int_{E_1}^{E_2} \left(\frac{\partial D}{\partial T}\right)_E \mathrm{d}E$ and adiabatic temperature change $\Delta T \approx -\int_{E_1}^{E_2} \frac{T}{\rho C_E}\left(\frac{\partial D}{\partial T}\right)_E \mathrm{d}E$ are induced when an electric field changes between $E_1$ and $E_2$.[15] In these equations, $T$ is the temperature in Kelvin scale, $\rho$ is the mass density, $C_E$ is the specific heat and $\partial D/\partial T$ is the pyroelectric coefficient. For dielectric materials, $D = \varepsilon_o\varepsilon_r E$, where $\varepsilon_o = 8.85 \times 10^{-12}$ C Vm$^{-1}$ the permittivity of the vacuum and $\varepsilon_r$ is the relative dielectric permittivity of the material. In the case of a non-adiabatic system, the difference between the electric field E induced and the zero field para-electric–ferroelectric transition temperatures $\Delta T = T_{P–F}(E) - T_{P–F}(0)$ can also be called ECE induced temperature change, although the actual temperature may not change considerably in absence of Joule heat.

In ferroelectric materials with spontaneous polarization $P_o$, $D = P_o + \varepsilon_o\varepsilon_r E$. EC effects are characterized by the EC responsivity $\frac{\Delta T}{E}$ (Km V$^{-1}$), the specific isothermal entropy change $\Delta s = \frac{\Delta s}{m}$ J (kg K)$^{-1}$, and the product of the adiabatic temperature change and specific isothermal entropy change $\Delta T\Delta s$ J kg$^{-1}$. Among organic solid EC materials, the typical values are $\frac{\Delta T}{E} \leq 10^{-7}$ Km V$^{-1}$, $\Delta s \sim 60$ J kg$^{-1}$ K$^{-1}$ and $\Delta T\Delta s < 1$ kJ kg$^{-1}$.[10] The highest reported value of $\Delta T\Delta s = 2.15$ kJ kg$^{-1}$ was observed in the relaxor ferroelectric $Pb_{0.8}Ba_{0.2}ZrO_3$ (PBZ) thin films,[16] high energy electron-irradiated polyvinylidene fluoride-trifluoroethylene relaxor copolymer and La-doped $PbZrTiO_3$ relaxor ceramic thin films.[17]

[a] *Advanced Materials and Liquid Crystal Institute, Kent State University, Kent, OH, 44242, USA. E-mail: ajakli@kent.edu; Tel: +1 330 672 4886; Web: https://media.kent.edu/~ajakli/E*
[b] *Materials Science Graduate Program, Kent State University, Kent, OH, 44242, USA*
[c] *Department of Physics, Kent State University, Kent, OH, 44242, USA*
[d] *Department of Chemistry and Biochemistry, Kent State University, Kent, OH 44242, USA*

† Electronic supplementary information (ESI) available. See DOI: https://doi.org/10.1039/d4sm00979g

Liquid crystals (LCs), which are used in displays, are anisotropic dielectric fluids, in which orientation of the anisotropic molecules can be easily modulated by a wide range of voltages with long operation life. These features make LCs promising candidates for realizing large ECE. In particular, large ECE were observed in LCs with large dielectric anisotropy near the isotropic (I)–nematic (N)[18–20] and isotropic–smectic phases[21–23] and in the transition to ferroelectric chiral smectic (SmC*) phases.[24] At the I–N transition, $\Delta T\Delta s \sim 100$ J kg$^{-1}$ was found, although they require up to 90 V μm$^{-1}$ fields to reach less than 1 mC m$^{-2}$ induced polarization.[18] During the transition to the SmA or SmC* phases, the EC responsivity values were $\frac{\Delta T}{E} \leq 10^{-7}$ Km V$^{-1}$ with typically $\Delta T < 1$ K and $E > 10$ V μm$^{-1}$. ECE in liquid crystals was also recently reviewed by Klemencic *et al.*[25]

Recently, an extraordinary new state of matter, namely, ferroelectric nematic liquid crystals (FNLC), was discovered.[26–33] Fluid FNLCs exhibit a large $>1$ *nC*/*N* piezoelectric coupling constant[34] and $\sim$50 mC m$^{-2}$ spontaneous electric polarization that is switchable well below 1 V μm$^{-1}$ field.[30,33] Szydlowska *et al.*[35] have studied an FNLC material with isotropic–nematic (N)–ferroelectric nematic ($N_F$) transition and found that the N–$N_F$ transition temperature can be shifted by 20 °C under 10 V μm$^{-1}$ DC electric fields corresponding to an EC responsivity of $2 \times 10^{-6}$ km V$^{-1}$. Unfortunately, other characteristics of ECE were not studied and no $\Delta s$ and $\Delta T\Delta s$ values were reported.

Herein, we investigated the ECE of a newly synthesized FNLC material, namely, PN03155, at the direct isotropic to ferroelectric nematic phase transition. The synthesis, molecular structure, chemical characterization, experimental methods, DSC scans and polarized optical microscopy (POM) textures are described in Fig. S1, S2–S5, S6, S7 and S8, respectively, of the ESI.† According to DSC scan results, the material had a direct isotropic to ferroelectric nematic ($N_F$) phase transition (corresponding to the paraelectric (P)–ferroelectric (F) transition described above) on cooling at 69.3 °C that persisted in room temperature. The I–$N_F$ transition followed first order kinetics; therefore, the isotropic phase could be overcooled by $\delta T$, and the transition occurred *via* nucleation of $N_F$ droplets in the isotropic phase, completing within the temperature range of $\leq \delta T$. On repeated measurements with the same cooling rates, the first $N_F$ droplets consistently (within 0.1 °C) appeared at the same temperature, but there were 0.1–0.3 °C temperature range differences for the completion of the transition. This is likely because the nucleation also depends on mechanical factors and noise. In spite of the competing Joule heat due to the relatively large ionic content of PN03155, we observed a large EC effect at unusually low electric fields ($\sim$1 V μm$^{-1}$).

## Results and discussion

The FNLC material PN03155 was filled in $d \approx 10$ μm thick cells, in which the glass substrates were coated with unidirectionally rubbed polyimide PI2555 that promotes planar alignment (average molecular axis parallel to the substrates) along the rubbing direction. Polarized optical microscopy (POM) images of cells are shown in Fig. 1 at 72 °C, where the first $N_F$ droplets appear on cooling from the isotropic phase. This indicates a transition temperature 2 °C higher than that observed during DSC studies, which might be due to the much slower cooling during the POM studies than during the DSC studies. Left column of Fig. 1(a, c and e) shows textures when no field is applied, and the right column of Fig. 1(b, d and f) shows textures when a field is applied on the LC.

The top row in Fig. 1(a and b) represents textures of a film with in-plane ITO electrodes separated by a 0.1 mm gap. As can be seen in Fig. 1(b), when a 75 V ($E$ = 0.75 V μm$^{-1}$) amplitude and $f$ = 40 Hz sinusoidal electric field was applied in between the in-plane electrodes, the material fully transitioned from the isotropic to the $N_F$ phase. This means that the energy barrier of the field helped in overcoming the specific enthalpy change of 4.4 J g$^{-1}$ that was observed in the DSC scans (see Fig. S7, ESI†). Notably, as long as the Joule heat arising due to the finite conductivity of the material can be neglected, the sample temperature does not change, and only the field-induced phase transition temperature, $\Delta T = T_{I\text{–}N_F}(E) - T_{I\text{–}N_F}(0)$, increases, which means this can be considered as an electrocaloric (EC) effect. The existence of EC effect was further evidenced by the textural changes under $E$ = 0.8 V μm$^{-1}$ and $f$ = 100 Hz sinusoidal electric field applied between indium tin oxide (ITO)-coated

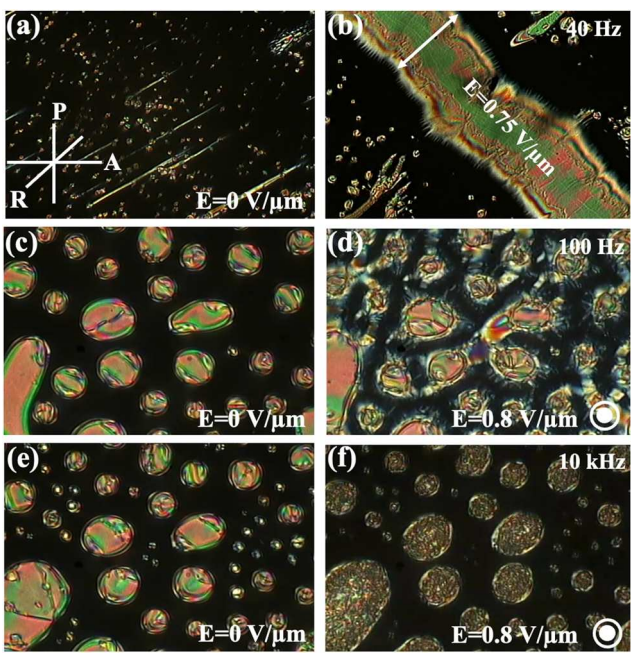


Fig. 1 Polarized optical microscopy (POM) images of 10 μm thick sandwich cells with in-plane (a) and (b) and between planes (c)–(f) field geometries at 72 °C. Left column (a), (c) and (e): No field applied; right column (b): $E$ = 0.75 V μm$^{-1}$, $f$ = 40 Hz sinusoidal electric field applied in between in-plane electrodes separated by a 0.1 mm gap; (d): $E$ = 0.8 V μm, $f$ = 100 Hz sinusoidal electric field applied in between indium tin oxide (ITO)-coated glass substrates; (f): $E$ = 0.8 V μm$^{-1}$, $f$ = 10 kHz sinusoidal electric field applied in between indium tin oxide (ITO)-coated glass substrates.

glass substrates. As seen in Fig. 1(c and d), the area of the birefringent $N_F$ domains increases upon applying the field, in contrast to the in-plane field, where the $N_F$ phase does not fill the entire area.

We qualitatively tested and observed that there are no significant differences in the responses below a frequency of $f \sim 200$ Hz, where $f < 1/\tau \sim \frac{1}{0.005} s$. This is because in the applied electric field range of $0.5 < E$ V μm$^{-1}$, the switching time of the polarization is $\tau < 5$ ms. For this reason, the difference between Fig. 1(b) and (d) is likely due to the appearance of the depolarization field $E_{dep} = -\frac{P_o}{\varepsilon_o \varepsilon}$ that acts against the applied field. The difference between the ITO-coated glass substrates under $E = 0.8$ V μm$^{-1}$ fields at 100 Hz seen in Fig. 1(d) and that at 10 kHz shown in Fig. 1(f) is due to the large difference in the applied frequency. At 100 Hz, the polarization can follow the field, while at 10 kHz it cannot be switched; *i.e.*, the effect of the polarization disappears. Consequently, the size of the birefringence domains does not grow under such field and only the alignment of the $N_F$ domains change since the material only has dielectric interaction with the 10 kHz field. This also shows that ferroelectric polarization is needed for the EC effect to be produced under such a low electric field.

Fig. 2 shows the temperature dependence of the average transmittance of a 10 μm cell under white light illumination at zero field between 72 °C and 70 °C using a sandwich (out-of-plane) cell. As seen in the main pane, the transmittance is $T = 0$ at 72.2 °C reaches $T = 1.9$ in arbitrary units at 72 °C, and then increases continuously to $T = 4.5$ at 70 °C. As shown in inset (a) of Fig. 2, upon applying a DC voltage $U$ at 72 °C, the transmittance decreases to basically zero under $U = 1.2$ V applied between the ITO substrates. This is due to the Joule heat $Q = \frac{U^2}{R} \cdot t$ that in time $t$, heats the material to the isotropic phase. Here, $R$ is the finite resistance $R = \frac{d}{\sigma \cdot A}$ of the cell, where $d \approx 10$ μm is the film thickness, $A \approx 1$ cm$^2$ is the area of the film, and $\sigma$ is the electric conductivity of the material. On the other hand, when 100 Hz AC voltage is applied, the transmittance increases from $T = 1.9$ at $U = 0$ V up to $T = 4.5$ at $U = 12$ V ($E = 1.2$ V μm$^{-1}$), and then, it decreases to $T = 0.6$ at $U = 22$ V (see inset (b) of Fig. 2). The increasing transmittance is clearly due to the ECE. Comparing the $E = 1.2$ V μm$^{-1}$ of the AC field-induced highest transmittance to the temperature-dependent zero field transmittance, we found that it corresponds to the zero-field transmittance at 70 °C. This meant an increase in $\Delta T \approx 2$ K of the I–$N_F$ phase transition temperature under $E = 1.2$ V μm$^{-1}$ electric field. This increase happened in spite of the increasing Joule heat that takes over the ECE at $E > 1.2$ V μm$^{-1}$. Comparing the transmittance values measured at different voltages at 72 °C and those measured at different temperatures at zero field, we constructed the $\Delta T(E)$ function as shown in inset (c) of Fig. 2.

The inset of Fig. 3 shows the temperature dependence of the ferroelectric polarization[36] (with values plotted against the left axis (brown triangle)) and of the threshold field required to fully switch the polarization at 80 Hz (triangular wave voltages plotted against the right axis (blue circle)). The polarization increases from zero at 72.2 °C, where the first $N_F$ domains appear, and increases sharply reaching the value of 2.9 μC cm$^{-2}$ at 69 °C, where the $N_F$ domains cover the entire volume. Simultaneously, the threshold field for polarization switching increases from 0.15 V μm$^{-1}$ at 70 °C up to 0.75 V μm$^{-1}$ at 50 °C. The plot in the main pane of Fig. 3 shows the electric field dependence of the measured polarization values at temperatures below the I–$N_F$ phase transition. In the 0.2–0.3 V μm$^{-1}$ range, the measured polarization stays close to zero at 72 °C as the transition to the $N_F$ phase shown in Fig. 1b needed a field of

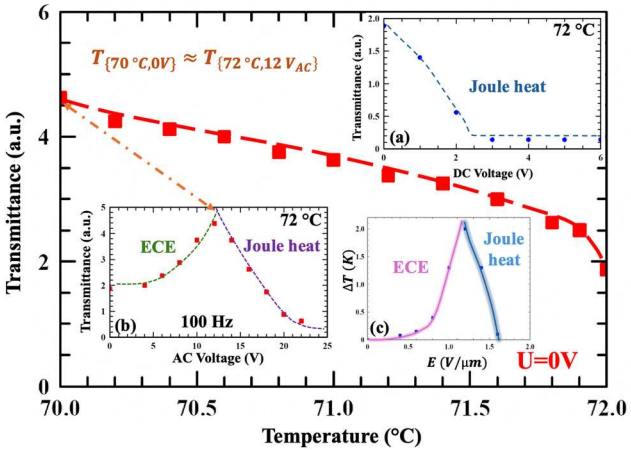


Fig. 2 Main pane: Temperature-dependent transmittance in arbitrary units of a 10 μm PN03155 film. Inset (a): DC field dependence of the transmittance at 72 °C. Inset (b): 100 Hz AC field dependence of the transmittance at 72 °C. Inset (c): Construction of the 100 Hz AC electric field dependence of $\Delta T$ by comparing the temperature dependences of the $U = 0$ V transmittance shown in the main pane and of the AC voltage dependent transmittance values shown in inset (b).

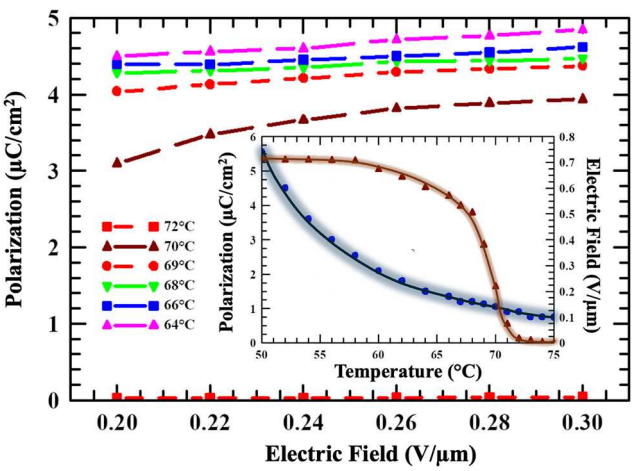


Fig. 3 Electric field dependence of the measured polarization values at various temperatures. Inset: Temperature dependence of the spontaneous polarization (left axis, brown triangle) and of the threshold voltage needed for full switching (right axis, blue circle). The width of the glow represents the measurement error.

over 0.4 V $\mu m^{-1}$ as seen in inset (b) of Fig. 2. At temperatures between 64 and 70 °C, the polarization increases with the applied electric field. Notably, for $T < 70$ °C, the $N_F$ phase is completely formed; *i.e.*, the measurement is performed in the single-phase $N_F$. In contrast to measurements at $T > 70$ °C where the I–$N_F$ transition is induced by ECE, in the completely formed $N_F$ phase we only increase the polar order. In particular, the increase in the zero-field polarization toward lower temperatures, as seen in the inset, is also due to the increase in the polar order (decrease of the director fluctuation). Therefore, the field-induced increase in the polar order can also be interpreted as a field-induced increase in the I–$N_F$ transition temperature $\Delta T = T_{I-N_F}(E) - T_{I-N_F}(0)$ as a consequence of the ECE.

The results presented in Fig. 2 allow us to quantify the ECE of the ferroelectric nematic liquid crystal PN03155 in terms of the EC responsivity $\frac{\Delta T}{E}(\mathrm{K\,m\,V})^{-1}$, specific isothermal entropy change $\Delta s = \frac{\Delta s}{m}$ (J (kg K)$^{-1}$), and product of the ECE temperature change and specific isothermal entropy change $\Delta T \Delta s$ J kg$^{-1}$. The observed $\Delta T \approx 2$ K under 1.2 V $\mu m^{-1}$ gives an EC responsivity of $\approx 1.7 \times 10^{-6}$ K m V$^{-1}$, which is in an order of magnitude larger than that found in organic solids, N and SmA liquid crystals and about the same as that calculated for another ferroelectric nematic LC material.[35] This large EC responsivity is mainly due to the extremely low field required for the switching of the ferroelectric polarization. The specific isothermal entropy change can be calculated from the specific transition enthalpy $H \approx 4.4$ J g$^{-1}$ = $T\Delta s$, giving $\Delta s \approx \frac{4400\ \mathrm{J\,kg^{-1}}}{(273+72)\mathrm{K}} \approx 13\ \mathrm{J\,(kg\,K)^{-1}}$ and $\Delta T \Delta s \approx 26$ J kg$^{-1}$. Although the obtained $\Delta T \Delta s$ value is ~3 times smaller than that found in dielectric LCs[18] at the I–$N_F$ transition, its required field is over 100 times smaller.[18]

Finally, we also found that the experimentally observed EC responsivity corresponds to a value that can be calculated from the electric analogy of the Clausius–Clapeyron equation, which relates the pressure-dependent slope of the melting temperature d$T$/d$p$, the specific enthalpy $H$ (obtained from DSC measurement shown in Fig. S7, ESI†), and the specific volume change $\Delta v$ at the phase transition temperature $T$ as $\frac{\mathrm{d}T}{\mathrm{d}p} = \frac{T \cdot \Delta v}{H}$. Replacing the specific work of the pressure $\mathrm{d}p \cdot \Delta v$ with the specific electrical energy $\left(PE + \frac{1}{2}\varepsilon_o \varepsilon E^2\right) \Big/ \rho$, where the first term is the ferroelectric, the second term is the dielectric specific energy density, and $\rho$ is the mass density, we arrive at the equation $\frac{\Delta T}{T} = \frac{PE + \frac{1}{2}\varepsilon_o \varepsilon E^2}{\rho \Delta H}$. Taking the polarization value $P \approx 0.03$ C m$^{-2}$ (see the inset to Fig. 3) when the ferroelectric nematic phase is completely formed at $T \approx 70$ °C $\approx 343$ K, mass density of $\rho \approx 1.3 \times 10^3$ kg m$^{-3}$, $H \approx 4.4 \times 10^3$ J kg$^{-1}$ and electric field $E = 1.2 \times 10^6$ V m$^{-1}$, and neglecting the dielectric term, the value of $\Delta T \approx 2.1$ K is obtained. This agrees well with the experimentally observed $\Delta T \approx 2.0$ K. Although in the isotropic phase, only dielectric coupling with the electric field is generally expected, to attain the observed $\Delta T \sim 2$ °C at $E = 1.2$ V $\mu m^{-1}$, this coupling would require a dielectric constant of $\varepsilon \sim 5 \times 10^3$, which is clearly too large for the isotropic phase. Hence, we conclude that the polar interaction we assumed was valid because in the temperature range wherein the ECE was observed, the material was overcooled and the ferroelectric phase was thermodynamically more stable.

To summarize, we described and quantitatively characterized the electrocaloric effect of a newly synthesized ferroelectric nematic liquid crystal compound (PN03155) at the isotropic–ferroelectric nematic (I–$N_F$) phase transition. While in DC field, the Joule heat completely suppressed the ECE, at $f \geq 40$ Hz harmonic AC fields, the ECE dominated below 1 V $\mu m^{-1}$ field with an EC responsivity of $\sim 1.7 \times 10^{-6}$ km V$^{-1}$. Although the product of the adiabatic temperature change and specific isothermal entropy change $\Delta T \Delta s \approx 26$ J kg$^{-1}$ was three times smaller than that found in dielectric LCs[18] at the I–N transition, the required field was over 100 times smaller. The EC effect under such low fields is a unique property of ferroelectric nematic liquid crystals. Although one may argue that AC fields are useless as there is no time for heat to flow after applying and removing the field, we found that the polarity of the field induced the shift in phase transition as long as the frequency of the field was low enough to fully switch the polarization. Therefore, heat flow was removed upon turning off the field and not during the polarity reversal. Additionally, we found that the obtained $\Delta T \Delta s$ values could be increased considerably by reducing the ionic content, thus suppressing the Joule heat.

## Data availability

The raw data of our manuscript entitled ''Low Field Electrocaloric Effect at Isotropic – Ferroelectric Nematic Liquid Transition'' by Adaka *et al.* will be made available by the corresponding author upon reasonable request.

## Conflicts of interest

There are no conflicts to declare.

## Acknowledgements

This work was financially supported by the US National Science Foundation grant DMR-2210083. We thank Professors S. Sprunt and J. Gleeson at the Kent State University for the useful discussions.

## References

1 J. Z. Hao, F. X. Hu, Z. B. Yu, F. R. Shen, H. B. Zhou, Y. H. Gao, K. M. Qiao, J. Li, C. Zhang, W. H. Liang,

J. Wang, J. He, J. R. Sun and B. G. Shen, *Chin. Phys. B*, 2020, **29**, 047504.
2 M. M. Vopson, *J. Phys. D: Appl. Phys.*, 2013, **46**, 345304.
3 I. N. Flerov, E. A. Mikhaleva, M. V. Gorev and A. V. Kartashev, *Phys. Solid State*, 2015, **57**, 429–441.
4 A. Gschneidner, V. K. Pecharsky and A. O. Tsokol, *Rep. Prog. Phys.*, 2005, **68**, 1479–1539.
5 A. S. Mischenko, Q. Zhang, J. F. Scott, R. W. Whatmore and N. D. Mathur, *Science*, 2006, **311**, 1270–1271.
6 L. Mañosa, D. González-Alonso, A. Planes, M. Barrio, J. L. Tamarit, I. S. Titov, M. Acet, A. Bhattacharyya and S. Majumdar, *Nat. Commun.*, 2011, **2**, 595.
7 M. S. Gruzdev, V. V. Korolev, A. G. Ramazanova, U. V. Chervonova and O. V. Balmasova, *Liq. Cryst.*, 2018, **45**, 907–911.
8 G. Skačej, *Liq. Cryst.*, 2018, **45**, 1964–1969.
9 J. Cui, Y. Wu, J. Muehlbauer, Y. Hwang, R. Radermacher, S. Fackler, M. Wuttig and I. Takeuchi, *Appl. Phys. Lett.*, 2012, **101**, 073904.
10 Z. Kutnjak, B. Rožič and R. Pirc, *Wiley Encyclopedia of Electrical and Electronics Engineering*, Wiley, 2015, pp. 1–19.
11 R. I. Epstein and K. J. Malloy, *J. Appl. Phys.*, 2009, **106**, 064509.
12 Y. S. Ju, *J. Electron. Packag*, 2010, **132**, 041004.
13 H. Gu, X. Qian, X. Li, B. Craven, W. Zhu, A. Cheng, S. C. Yao and Q. M. Zhang, *Appl. Phys. Lett.*, 2013, **102**, 122904.
14 C. Aprea, A. Greco, A. Maiorino and C. Masselli, *J. Phys.: Conf. Ser.*, 2017, **796**, 012019.
15 B. Neese, B. Chu, S.-G. Lu, Y. Wang, E. Furman and Q. M. Zhang, *Science*, 2008, **321**, 821–823.
16 B. Peng, H. Fan and Q. Zhang, *Adv. Funct. Mater.*, 2013, **23**, 2987–2992.
17 S. G. Lu, B. Rožič, Q. M. Zhang, Z. Kutnjak, X. Li, E. Furman, L. J. Gorny, M. Lin, B. Malič, M. Kosec, R. Blinc and R. Pirc, *Appl. Phys. Lett.*, 2010, **97**, 162904.
18 X. S. Qian, S. G. Lu, X. Li, H. Gu, L. C. Chien and Q. Zhang, *Adv. Funct. Mater.*, 2013, **23**, 2894–2898.
19 I. Lelidis and G. Durand, *Phys. Rev. Lett.*, 1996, **76**, 1868–1871.
20 X.-S. Qian, S. G. Lu, X. Li, H. Gu, L.-C. Chien, Q. M. Zhang, L.-C. Chien, Q. M. Zhang, L.-C. Chien and Q. M. Zhang, *MRS Proc.*, 2013, **1543**, 13–20.
21 M. Trèek, M. Lavriè, G. Cordoyiannis, B. Zalar, B. Rožič, S. Kralj, V. Tzitzios, G. Nounesis and Z. Kutnjak, *Philos. Trans. R. Soc., A*, 2016, **374**, 20150301.
22 D. Črešnar, N. Derets, M. Trček, G. Skačej, A. Rešetič, M. Lavrič, V. Domenici, B. Zalar, S. Kralj, Z. Kutnjak and B. Rožič, *J. Phys. Energy*, 2023, **5**, 045004.
23 E. Klemenčič, M. Trček, Z. Kutnjak and S. Kralj, *Sci. Rep.*, 2019, **9**, 1721.
24 E. Bsaibess, A. Hadj Sahraoui, Y. Boussoualem, M. Soueidan, B. Duponchel, D. P. Singh, B. Nsouli, A. Daoudi and S. Longuemart, *Liq. Cryst.*, 2019, **46**, 1517–1526.
25 E. Klemencic, M. Trcek, Z. Kutnjak and S. Kralj, *Electrocaloric Effect*, 2023, 205–223.
26 R. J. Mandle, S. J. Cowling and J. W. Goodby, *Phys. Chem. Chem. Phys.*, 2017, **19**, 11429–11435.
27 A. Mertelj, L. Cmok, N. Sebastián, R. J. Mandle, R. R. Parker, A. C. Whitwood, J. W. Goodby and M. Čopič, *Phys. Rev. X*, 2018, **8**, 041025.
28 N. Sebastián, L. Cmok, R. J. Mandle, M. R. De La Fuente, I. Drevenšek Olenik, M. Čopič and A. Mertelj, *Phys. Rev. Lett.*, 2020, **124**, 037801.
29 R. J. Mandle, N. Sebastián, J. Martinez-Perdiguero and A. Mertelj, *Nat. Commun.*, 2021, **12**, 4962.
30 H. Nishikawa, K. Shiroshita, H. Higuchi, Y. Okumura, Y. Haseba, S. Yamamoto, K. Sago and H. Kikuchi, *Adv. Mater.*, 2017, **29**, 1702354.
31 R. J. Mandle, S. J. Cowling and J. W. Goodby, *Chem. – Eur. J.*, 2017, **23**, 14554–14562.
32 N. Sebastián, M. Čopič and A. Mertelj, *Phys. Rev. E*, 2022, **106**, 021001.
33 X. Chen, E. Korblova, D. Dong, X. Wei, R. Shao, L. Radzihovsky, M. A. Glaser, J. E. Maclennan, D. Bedrov, D. M. Walba, N. A. Clark, N. L. Abbott, P. Palffy-Muhoray and P. Pieranski, A. contributions, N. designed research, N. performed research and N. analyzed data, *Proc. Natl. Acad. Sci. U. S. A.*, 2020, **117**, 14021–14031.
34 M. T. Máthé, M. S. H. Himel, A. Adaka, J. T. Gleeson, S. Sprunt, P. Salamon and A. Jákli, *Adv. Funct. Mater.*, 2024, 2314158.
35 J. Szydlowska, P. Majewski, M. Čepič, N. Vaupotič, P. Rybak, C. T. Imrie, R. Walker, E. Cruickshank, J. M. D. Storey, P. Damian and E. Gorecka, *Phys. Rev. Lett.*, 2023, **130**, 216802.
36 K. Miyasato, S. Abe, H. Takezoe, A. Fukuda and E. Kuze, *Jpn. J. Appl. Phys.*, 1983, **22**, L661–L663.

 